As in finite element analysis, depending on the admissible functions selected, the generalized coordinates become discrete coordinates, like nodal displacements, nodal slopes, or nodal strains. (In finite element analysis, the discretized equations governing the motion of the structure are obtained by minimizing a weighted residual. Depending on the admissible functions selected, the discretized coordinates become nodal displacements, nodal angles, etc.) The numerical illustration given in the next section clarifies this point.

Numerical Illustration

Consider a simple pinned-pinned beam of length L undergoing bending vibration. The uniform bending operator is $L(\,) = EI\,\mathrm{d}^4(\,)/\mathrm{d}x^4$, and the beam's associated natural modes of vibration and natural frequencies of oscillation are given by $\phi_r(x) = (2/\rho L)^{1/2}\sin(r\pi x/L)$ and $\omega_r = r\pi(EI/\rho L^4)^{1/2}$, respectively. Assume that the beam is initially at rest and undeformed when a uniform gravity load is applied. For simulation purposes we assumed that 20 modes participate significantly in the overall system response.

The beam shall be controlled two ways: using distributed uniform damping and stiffening and using discrete uniform damping and stiffening (see Fig. 1). In the discrete case we shall let uniform damping and stiffening be realized using two discrete moments $F_1(t) = M_1(t)$ and $F_2(t) = M_2(t)$ at each end of the beam and using a discrete force $F_3(t) = F_C(t)$ in the center of the beam. The associated discrete measurements are two angular displacement measurements $U_1(t) = \theta_1(t)$ and $U_2(t) = \theta_2(t)$ at each end of the beam and a displacement measurement $U_3(t) = U_C(t)$ in the center of the beam. The admissible functions $\varphi_r(x)$, $(r = 1, 2, 3)$ that turn the generalized forces and measurements into these discrete forces and measurements are determined from Eq. (9) to be

$$\varphi_1(x) = L\left[-\tfrac{3}{8} + (x/L) - \tfrac{1}{2}(x/L)^2\right]$$

$$\varphi_2(x) = L\left[-\tfrac{1}{8} + \tfrac{1}{2}(x/L)^2\right], \qquad \varphi_3(x) = 1$$

The discrete control forces are expressed as a distributed force as

$$f_{\mathrm{CD}}(x,t) = -M_1(t)\frac{\mathrm{d}[\delta(x-0)]}{\mathrm{d}x} - M_2(t)\frac{\mathrm{d}[\delta(x-L)]}{\mathrm{d}x} + F_C(t)\delta\left(\frac{x-L}{2}\right)$$

The displacements in the center of the beam using distributed uniform damping and uniform stiffening are shown in Fig. 2. The displacements in the center of the beam and the associated time-lapse plots using discrete uniform damping and uniform stiffening are shown in Figs. 3 and 4. Comparing the distributed control with the discrete control, notice that the discretization errors associated with vibration damping and uniform stiffening are indistinguishable, whereas the discretization error associated with the damping of the steady-state error is significant. The discretization error associated with the steady-state error is significant because the steady-state error is not completely controllable (cannot be completely removed) regardless of the control gains.

Conclusions

This Note extends the uniform vibration damping results of Ref. 4 in two directions. First, uniform damping of the steady-state error and uniform stiffening of the structural vibration together with the uniform damping of the vibration were shown to lead to a localized control algorithm, like uniform vibration damping alone. This result was articulated in a Uniform Damping and Uniform Stiffening Principle stating that the associate "control algorithm is fully localized—the control force depends only on local measurements and on local physical parameters (ρ and $\boldsymbol{L}$)." Secondly, a general weighted-residual method was developed for the discretization of the distributed forces into discrete forces. The method was illustrated in a numerical example.

Acknowledgments

The work by Larry Silverberg was supported in part by the Mars Mission Research Center, NASA Grant NAGW-1331, and the North Carolina Space Grant Consortium, NASA Grant NGT5-40011. The work by Gregory Washington was supported in part by ARO Grant DAAG5-98-1-0498.

References

[1] Meirovitch, L., and Baruh, H., "Control of Self-Adjoint Distributed-Parameter Systems," *Journal of Guidance, Control, and Dynamics*, Vol. 1, No. 1, 1982, pp. 60–66.

[2] West-Vukovich, G. S., Davison, E. J., and Hughes, P. C., "The Decentralized Control of Large Flexible Space Structures," *IEEE Transactions on Automatic Control*, Vol. AC-29, No. 10, 1984, pp. 866–879.

[3] Kirk, D. E., *Optimal Control Theory*, Prentice–Hall, Englewood Cliffs, NJ, 1970

[4] Silverberg, L., "Uniform Damping Control of Spacecraft," *Journal of Guidance, Control, and Dynamics*, Vol. 9, No. 2, 1986, pp. 221–227.

[5] Meirovitch, L., *Principles and Techniques of Vibrations*, Prentice–Hall, Englewood Cliffs, NJ, 1997.

[6] Meirovitch, L., and Silverberg, L., "Globally Optimal Control of Self-Adjoint Distributed Systems," *Journal of Optimal Control, Applications, and Methods*, Vol. 4, 1983, pp. 365–386.

[7] Silverberg, L., Redmond, J. M., and Weaver, L., "Uniform Damping Control: Discretization and Optimization," *Applied Mathematical Modeling*, Vol. 16, March 1992, pp. 133–140.

[8] Washington, G. N., and Silverberg, L., "Uniform Damping and Stiffness Control of Distributed Systems," *ASME Journal of Dynamic Systems, Measurement, and Control*, Vol. 119, No. 3, 1997, pp. 561–565.

Horizontal Control Effector Sizing for Supersonic Transport Aircraft

Eric Hallberg* and Isaac Kaminer†
Naval Postgraduate School, Monterey, California 93943

I. Introduction

THE use of an automatic flight augmentation system is commonplace on a modern aircraft. Its benefits include alleviation of undesirable flight characteristics, reduction of pilot workload, and increase in performance and fuel efficiency. Therefore, feedback (dynamic) considerations should be included in determining the sizes of aircraft control surfaces. Traditionally, only static constraints have been used for control surface sizing. For example, in the case of a horizontal tail of a given volume, constraints are calculated that limit the fore and aft travel of the c.g. Constraints that limit the forward c.g. position include 1) sufficient nose-up pitch acceleration at the rotation speed (nose-wheel lift off) and 2) sufficient nose-up pitch acceleration at the approach speed in the landing configuration (go-around). Constraints that limit aft c.g. position include 1) at brake release with maximum thrust sufficient weight on the nose gear (tip back), 2) pitch-up acceleration at the rotation speed (nose-wheel lift off), and 3) sufficient nose-down pitch acceleration at minimum flying speeds.[1] However, for the aft c.g. locations at the approach flight condition of a supersonic transport aircraft, dynamic constraints may be more restrictive than the static ones.

Received 11 May 1998; revision received 28 January 1999; accepted for publication 3 February 1999. This paper is declared a work of the U.S. Government and is not subject to copyright protection in the United States.

*Lt. Commander, U.S. Navy, Department of Aeronautical and Astronautical Engineering.

†Associate Professor, Department of Aeronautical and Astronautical Engineering. Member AIAA.

This Note extends the results in Ref. 1, where preliminary work on horizontal tail sizing for a supersonic transport aircraft using dynamic constraints is reported. However, the issue of using actuator rate constraints in the tail-sizing process was not explicitly addressed. Furthermore, we adopt a numerical solution similar to the one introduced in Ref. 2, where an integrated aircraft controller design methodology using linear matrix inequalities (LMIs) was applied to the control power sizing for an F–14 aircraft. The major contribution of this Note is twofold.

First, the tail-sizing design problem is defined in terms that include the integral participation of a feedback control system. Because the degree of control of the longitudinal dynamics depends on how fast and far the longitudinal control surface(s) can be moved by the control actuator(s), we show that a natural metric to capture the *size* of the automatic flight control system is the maximum actuator rate. Using this metric allows for design tradeoffs that inherently include considerations of actuator performance. For instance, it may be more cost effective to incorporate faster, generally larger and more expensive actuators rather than pay the drag penalty associated with a larger horizontal tail.

To state the second contribution of this Note we need the follwing definitions. First, as a measure of the horizontal tail size we will use the tail volume defined as a ratio between the product of the tail area and distance between aerodynamic centers of the tail and wing body and the product of the wing area and mean aerodynamic cord. Second, we need to define the tail-sizing design space. The tail-sizing design space is the region of acceptable combinations of tail volume $\bar{V}_H$, c.g. station $x_{\text{c.g.}}$, and peak actuator rate $\dot{u}_{\max}$. The triplet $(\bar{V}_H, x_{\text{c.g.}}, \dot{u}_{\max})$ defines an aircraft model and an automatic flight control system. The model is obtained through the linearization of the nonlinear dynamics of the supersonic transport aircraft at an equilibrium point. It is partially defined by the specified tail volume and c.g. position. The automatic flight control system is characterized by the specified maximum actuator rate in the triplet. By acceptable it is meant that, for the model associated with the triplet $(\bar{V}_H, x_{\text{c.g.}}, \dot{u}_{\max})$, a linear controller is known to exist that 1) stabilizes the plant, 2) meets prescribed dynamic performance constraints, and 3) does not exceed the maximum actuator rate and amplitude constraints in response to a given disturbance (dynamic constraint).

Now, the second contribution of this Note is a development of a numerical tool that, for a given aircraft dynamic model, flight condition, and dynamic constraint, determines the tail-sizing design space. This tool is termed the tail-sizing design tool and provides the user with the capability to measure the effect of adding a second horizontal control surface in the form of a canard as well as the capability to measure the effect of simple, symmetric, flexible motion of the vehicle on the tail-sizing design space. Based on numerical analysis of designs, canards are shown to disproportionatelyaid the control problem, especially in countering the detrimental effects of aeroelastic motion.

The Note is organized as follows. Section II discusses model development for a rigid-body supersonic transport aircraft with and without canards. Section III uses the LMI developed in Ref. 3 to formulate the plant controller optimization problem that is the key element of the tail-sizing design tool and is used to obtain the tail-sizing design space. The dynamic constraint associated with this problem is the recovery from a severe angle-of-attack excursion without exceeding actuator amplitude and rate constraints. Numerical results are reported in Sec. IV based on the application of the tail-sizing design tool to a rigid-body supersonic transport model representative of current designs. Section V presents numerical results obtained by applying the tail-sizing design tool to an aeroelastic supersonic transport model.

II. Development of a Rigid-Body Model

Let x_{cg} denote the c.g. location as a fraction of the reference chord, and let x denote the vector of four longitudinal states, consisting of forward and down components of the airspeed vector and of the aircraft's pitch and pitch rate. Let u_h denote the horizontal tail incidence angle, and let $\bar{V}_H$ denote the tail volume defined using the distance from the wing-body aerodynamic center to the tail aerodynamic center. This representation is convenient because, for one flight condition, the wing-body mean aerodynamic center remains constant. Thus, the control surface volume and c.g. are decoupled in terms of their influence on the vehicle dynamics.

Typically, the longitudinal dynamics of the aircraft can be expressed by the following system of differential equations:

$$\mathcal{G} = \begin{cases} \dot{x} = \mathcal{F}(x, u_h, x_{\text{cg}}, \bar{V}_H) \\ z = \mathcal{H}(x, u_h) \end{cases} \tag{1}$$

where $\mathcal{F}(\cdot)$ is a C^1 function of $x, u_h, x_{\text{cg}}, \bar{V}_H$; $\mathcal{H}$ is a C^1 function relating x and z; and $z = [V_T \;\; \gamma]^T$ defines the true airspeed V_T and flight-path angle γ. Here the vector z is used to characterize a given flight condition. Let x_0, u_{h_0} denote the trim values of x and u_h for given z_0, c.g. location x_{cg}, and tail volume $\bar{V}_H$; then $\mathcal{F}(x_0, u_0, x_{\text{cg}}, \bar{V}_H) = 0$ and $\mathcal{H}(x_0, u_0) = z_0$.

Flying quality requirements are typically characterized by the level of attention and skill required of the pilot to control the aircraft. They are grouped in three levels. A lower numerical level corresponds to more benign flight characteristics. The problem formulation matches an acceptable region in the left half plane for the closed-loop eigenvalues of the linear model with flying qualities. Specifically, in order to achieve certain Level II flying qualities requirements, a necessary, although not sufficient, condition is for the eigenvalues of $\mathcal{G}_l$ to be placed in a region in the left half plane characterized as having a minimum damping ratio of 0.2 and damped natural frequency of 0.2 radians per second.

The horizontal tail is the most commonly used effector for longitudinal control of the aircraft. It is not uncommon, however, for long, slender aircraft designs to include canards for supplemental longitudinal control. The XB-70 and B-1B are two examples. The presence of the canards is usually attributed to flying quality control issues involving the flexible nature of these aircraft.[4] This point is addressed in a subsequent section concerning control of an aeroelastic aerodynamic model. To lay the groundwork for that section, and as a baseline point of comparison with a rigid structure, this section addresses the addition of a longitudinal control effector forward of the wing. The effect on the tail-sizing design space is explored when the feedback control system is free to utilize both control surfaces in order to recover from angle-of-attack excursions.

Revisions to the nonlinear equations of motion required to account for the addition of the canards parallel the development in Ref. 5 and have the following form:

$$\mathcal{G} = \begin{cases} \dot{x} = \mathcal{F}(x, u_h, u_c, x_{\text{cg}}, \bar{V}_H, \bar{V}_C) \\ z = \mathcal{H}(x, u_h, u_c) \end{cases} \tag{2}$$

where $\bar{V}_C$ and u_c denote the canard volume and incidence angle, respectively. When these nonlinear equations of motion are linearized about the equilibrium point determined by $(z_0, x_{\text{cg}}, \bar{V}_H, \bar{V}_C)$, the following linear time invariant system results:

$$\delta\dot{x} = A(z_0, x_{\text{cg}}, \bar{V}_H, \bar{V}_C)\delta x + B_c(z_0, x_{\text{cg}}, \bar{V}_C)\delta u_c + B_h(z_0, x_{\text{cg}}, \bar{V}_H)\delta u_h \tag{3}$$

Actuator dynamics for both the canard and horizontal tail were appended to the linearized longitudinal dynamics. Linear models of the following form were used to describe canard and tail actuator dynamics:

$$\dot{x}_a = \begin{bmatrix} A_{a_c} & 0 \\ 0 & A_{a_h} \end{bmatrix} x_a + \begin{bmatrix} B_{a_c} & 0 \\ 0 & B_{a_h} \end{bmatrix} \begin{bmatrix} \bar{u}_c \\ \bar{u}_h \end{bmatrix}$$

$$x_a = \begin{bmatrix} x_{a_c}^T & x_{a_h}^T \end{bmatrix}^T, \qquad u_c = C_{a_c} x_a, \qquad u_h = C_{a_h} x_a \tag{4}$$

$$\dot{u}_c = C_{r_c} x_a + D_{r_c} \bar{u}_c, \qquad \dot{u}_h = C_{r_h} x_a + D_{r_h} \bar{u}_h$$

where x_a, $\bar{u}_c$, and $\bar{u}_h$ denote canard and tail actuator states and canard and tail actuator inputs, respectively. Let the interconnection of the linearized plant and actuator dynamics be denoted by

$\mathcal{G}_l(z_0, x_{cg}, \bar{V}_H, \bar{V}_C)$. Now, for each design point $\mathcal{G}_l(z_0, x_{cg}, \bar{V}_H, \bar{V}_C)$ the question becomes the following: Is the set of feedback controllers that recover the aircraft from the angle-of-attack excursion, while maintaining acceptable flying qualities without saturating the actuator or exceeding a certain actuator rate, empty?

III. Numerical Solution Algorithm

The plant-controller optimization (PCO) problem to be solved in this section can be stated as follows: Let a flight condition be specified by the aircraft's flight speed, altitude, and flight-path angle. Furthermore, let a certain set of flying quality requirements be given for that flight condition. Define the dynamic constraint to be the recovery of the aircraft from a high angle-of-attack excursion, while not exceeding certain peak actuator rate and actuator amplitude limits. Then, for a range of horizontal tail volumes and peak actuator rates determine the aft c.g. limits for which there still exists a state-feedback controller that 1) stabilizes the feedback system, 2) satisfies the flying quality and dynamic requirements, and 3) meets actuator rate and amplitude constraints.

Clearly, when the plant parameters (tail and/or canard volume) and actuator limits are fixed the PCO problem can be formulated in terms of LMIs obtained in Ref. 3. The solution to this problem consists of the maximum allowable c.g. location for which a feasible controller still exists and of the controller itself. Now, by varying plant parameters and actuator constraints we obtain a set of maximum allowable c.g. locations and feasible controllers, parametrized by actuator constraints. The projection of this set onto a three-dimensional space spanned by tail volume, c.g. location, and actuator rate limit defines a surface in the tail-sizing design space that is extremely useful in the preliminary aircraft design. This process is detailed next.

Let $u_{h_{\max}}, \dot{u}_{h_{\max}}, u_{c_{\max}}, \dot{u}_{c_{\max}}$ denote maximum tail actuator amplitude and rate and maximum canard actuator amplitude and rate constraints, respectively. Let $\bar{A}$ and $\bar{B}$ denote the state and input matrices of the serial inter connection of systems (3) and (4), respectively. Furthermore, let $\phi = \cos^{-1}$ (minimum damping) and let β denote the minimum damped natural frequency. Define the following LMI feasibility set:

$$
\begin{aligned}
&\Phi_1\left[\mathcal{G}_l\left(Z_0, x_{cg_0}, \bar{V}_{H_0}, \bar{V}_{C_0}\right), u_{h_{\max}}, \dot{u}_{h_{\max}}, u_{c_{\max}}, \dot{u}_{c_{\max}}, \nu_0\right] \\
&= \left\{ W, Y > 0 : \begin{bmatrix} Y & Y^T\begin{bmatrix} 0 & C_{r_c} & 0 \end{bmatrix}^T + W^T\begin{bmatrix} D_{r_c} & 0 \end{bmatrix}^T \\ \begin{bmatrix} 0 & C_{r_c} & 0 \end{bmatrix} Y + \begin{bmatrix} D_{r_c} & 0 \end{bmatrix} W & \dot{u}_{c_{\max}}^2 \end{bmatrix} \geq 0, \begin{bmatrix} 1 & \nu_0^T \\ \nu_0 & Y \end{bmatrix} \geq 0, \right. \\
&\begin{bmatrix} Y & Y^T\begin{bmatrix} 0 & 0 & C_{r_h} \end{bmatrix}^T + W^T\begin{bmatrix} 0 & D_{r_h} \end{bmatrix}^T \\ \begin{bmatrix} 0 & 0 & C_{r_h} \end{bmatrix} Y + \begin{bmatrix} 0 & D_{r_h} \end{bmatrix} W & \dot{u}_{h_{\max}}^2 \end{bmatrix} \geq 0, \begin{bmatrix} 1 & \nu_0^T \\ \nu_0 & Y \end{bmatrix} \geq 0, \\
&\begin{bmatrix} (\sin\phi)(\bar{A}Y + \bar{B}W) + (\sin\phi)(\bar{A}Y + \bar{B}W)^T & -(\cos\phi)(\bar{A}Y + \bar{B}W) + (\cos\phi)(\bar{A}Y + \bar{B}W)^T & 0 \\ (\cos\phi)(\bar{A}Y + \bar{B}W) - (\cos\phi)(\bar{A}Y + \bar{B}W)^T & (\sin\phi)(\bar{A}Y + \bar{B}W) + (\sin\phi)(\bar{A}Y + \bar{B}W)^T & 0 \\ 0 & 0 & \bar{A}Y + \bar{B}W + (\bar{A}Y + \bar{B}W)^T + 2\beta Y \end{bmatrix} < 0, \\
&\left. \begin{bmatrix} Y & Y^T\begin{bmatrix} 0 & C_{a_c} & 0 \end{bmatrix}^T \\ \begin{bmatrix} 0 & C_{a_c} & 0 \end{bmatrix} Y & u_{c_{\max}}^2 \end{bmatrix} \geq 0, \begin{bmatrix} Y & Y^T\begin{bmatrix} 0 & 0 & C_{a_h} \end{bmatrix}^T \\ \begin{bmatrix} 0 & 0 & C_{a_h} \end{bmatrix} Y & u_{h_{\max}}^2 \end{bmatrix} \geq 0 \right\}
\end{aligned} \tag{5}
$$

Then, a sufficient condition for the existence of a static, state-feedback controller that stabilizes the feedback system $\mathcal{G}_l(Z_0, X_{cg_0}, \bar{V}_{H_0}, \bar{V}_{C_0})$, does not exceed actuator amplitude and rate limits, and results in acceptable flying qualities in response to the angle-of-attack excursion denoted by vector ν_0, is for the set Φ_1 to be nonempty. Here the LMIs (5) were obtained using the approach outlined in Ref. 3. Now, the PCO problem considered in this section can be stated as follows. For a given range of horizontal tail volumes and tail and canard actuator rate constraints,

Maximize $\{x_{cg}\}$, subject to

$$\mathcal{F}(x_0, u_0, x_{cg}, \bar{V}_H, \bar{V}_C) = 0, \qquad \mathcal{H}(x_0, u_0) = z_0$$

$$(Y, W) \in \Phi_1\left[\mathcal{G}_l(x_{cg}, \bar{V}_H, \bar{V}_C), u_{h_{\max}}, \dot{u}_{h_{\max}}, u_{c_{\max}}, \dot{u}_{c_{\max}}, \nu_0\right] \tag{6}$$

A solution to this PCO problem includes a set of feasible state-feedback controllers that stabilize the plant $\mathcal{G}_l(z_0, x_{cg}, \bar{V}_H, \bar{V}_C)$ and meet actuator limit requirements, as well as a set of corresponding maximum aft c.g. locations. The numerical solution used to map the tail-sizing design space involved a binary search over c.g. stations and was implemented in the tail-sizing design tool using the MATLAB™ LMI toolbox.[6]

IV. Results—Rigid-Body Model

In this section we present the results of applying the tail-sizing design tool to the aerodynamic model termed Ref A, which represents a modified XB-70 aircraft. See Appendix A in Ref. 3, where the details on the buildup of the nonlinear longitudinal dynamics in terms of wing-body and tail contributions for the Ref A model can be found.

The state-feedback synthesis LMIs (set Φ_1) were used. The data were obtained by the tail-sizing tool for a range of tail volumes from 0.1 to 0.3 and a range of peak actuator rates from 5 to 30 deg/s for the rigid-body model. Figure 1 shows the result of fitting a surface to this data set. The surface represents a lower bound on the peak actuator rate required by the feedback control system to recover from the angle-of-attack excursion, for various combinations of c.g. locations and tail volumes. An upper bound in the tail-sizing design space is given by a fixed limit on the peak actuator rate available. Figure 1 also shows the plane representing a peak actuator rate of 15 deg/s. The volume below the plane and above the curved surface represents the tail-sizing design space, where state-feedback controllers are known to exist that meet design requirements.

Next, a canard was added to the Ref A model with the volume fixed at 0.05. Following the procedure outlined earlier, the lower surface of the tail-sizing design space was mapped for a range of horizontal tail volumes from 0.1 to 0.3 and for a range of peak actuator rates from 5 to 30 deg/s. Amplitude and actuator rate limits for the canard and horizontal tail were matched. Figure 2 shows a slice of the two surfaces just calculated at a peak actuator rate limit of 15 deg/s. This should be familiar as a conventional scissors plot.[1] Of course, as one would expect, the design space increases with the additional control power available from the canard. The pertinent question is whether or not there is any benefit in spreading the control power fore and aft, so to speak, or if the tail-sizing design space would have increased just as much had the tail volume alone been increased by 0.05 and the canard not added. In general, it makes more sense to compare the competing configurations in terms of equal

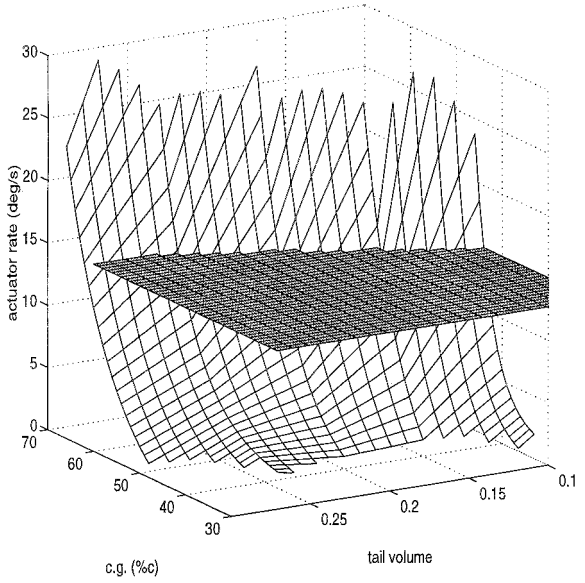

Fig. 1 Rigid-body model: three-dimensional tail-sizing design space with peak actuator rate limit.

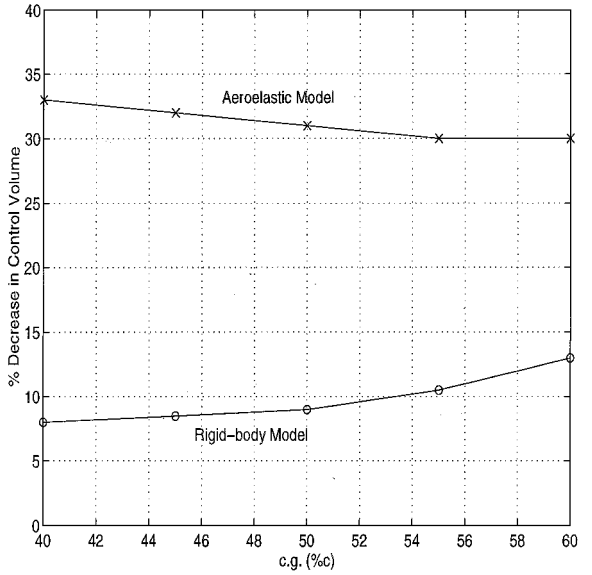

Fig. 3 Decrease in total control volume with the addition of canard for rigid and aeroelastic models.

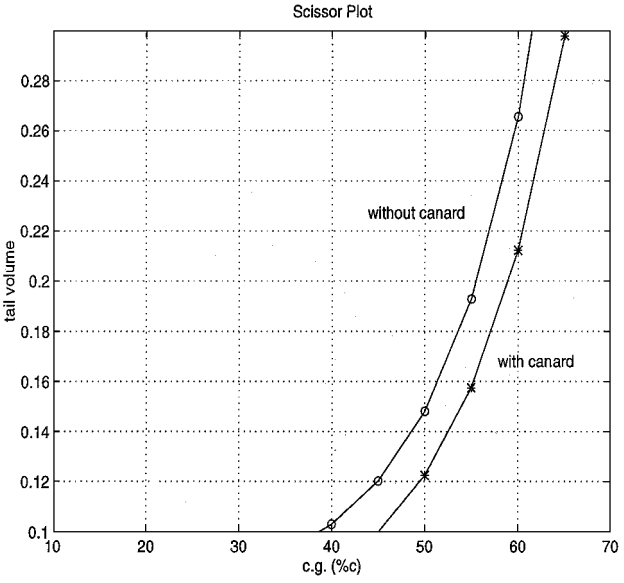

Fig. 2 Rigid-body model: two-dimensional slice of tail-sizing design space with and without a canard.

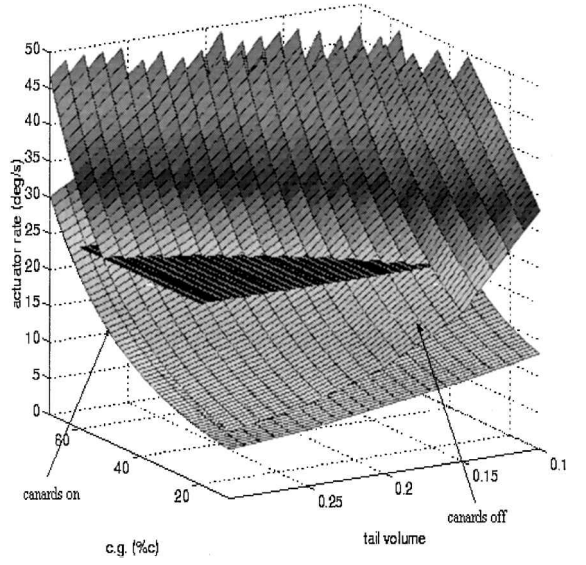

Fig. 4 Aeroelastic model: tail-sizing design space comparison, canard on and off.

amounts of combined horizontal tail and canard surface area. For instance, profile drag is more closely related to the surface area of the control surfaces, among other things, and the design goal might be to minimize drag for the same aft c.g. station and actuator rate limit. For this example, which utilized the Ref A data, the distance from the vehicle's wing-body neutral point to the aerodynamic center of the canard or horizontal tail was the same. Therefore, comparisons in terms of normalized area or volume are equivalent.

Figure 3 compares the two configurations, the first without a canard and the second with a canard. The percent change in total control volume required in going from a configuration without a canard to a configuration with a canard is shown as a function of the aft c.g. limit. The same flying quality requirements and actuator limits were used. For the rigid-body supersonic transport aircraft model the benefit gained from the inclusion of a canard is about a 10% savings in total control volume.

V. Results—Aeroelastic Model

The development of an aeroelastic aerodynamic model followed well-documented work by Waszak and Schmidt.[7] As a starting point, it utilized the same rigid-body stability and control derivatives as the Ref A model. The dynamics of the flexible mode and cross-coupling effects between rigid-body and flexible motion of the first, symmetric, flexible bending mode were incorporated in the model. In the sequel we shall refer to this aeroelastic model as Ref B (see Ref. 3). Qualitative differences between the two models are discussed next. Table 1 compares the eigenvalues of Ref A and B models. The frequency separation between the elastic mode and the short period dynamics is approximately 1 Hz, and the damping of the flexible mode is only 0.02. Typically, attempts are made to attenuate the feedback prior to excitation of the flexible dynamics. On large transport aircraft with the flexible dynamics close in frequency to the short period dynamics, this is hardly possible. Furthermore, even if suitable notch or low-pass filtering within the control loop could be attained, the extremely light damping of the flexible modes is problematic because of the gust-induced structural responses and fatigue life. Therefore, the problem posed will be one of actively controlling the flexible modes retained. Generally, this will entail improving the damping of the flexible dynamics while ensuring stability of the short period dynamics as the c.g. is moved aft.

Once again, the LMI-based tail-sizing design tool was used to study the effect of the addition of a canard to the aeroelastic model Ref B. As before, a canard volume of 0.05 was selected, and the design space was determined. Figure 4 compares the design space of the aeroelastic model with and without the canard and also includes a plane representing a constant peak actuator rate of 25 deg/s. Of

Table 1 Eigenvalues of aeroelastic and rigid-body models

	Short period		Long period		Flexible mode	
Model	Frequency, rad/s	Damping	Frequency, rad/s	Damping	Frequency, rad/s	Damping
Aeroelastic	0.90	0.75	0.14	0.55	6.7	0.02
Rigid body	0.91	0.75	0.14	0.07	n/a	n/a

course, the added control volume caused by the canard allows a further aft c.g. location for the same actuator rate limit.

The relative effect of adding a canard is addressed by comparing the total control volume ($\bar{V}_H + \bar{V}_C$) required for a given aft c.g. limit and peak actuator rate limit. The results are shown in Fig. 3 as a percent reduction in control volume required in going from the configuration without a canard to the configuration with a canard. Because the lengths of the tail and canard moment arms are the same, Fig. 3 also represents savings in total control effector volume. Experience has shown that the use of canards is desirable for flexible aircraft.[4] This method provides a metric to quantify that benefit. In this example the inclusion of a canard is 300% more effective when added to the aeroelastic model than when added to the rigid-body model.

VI. Conclusions

For statically unstable aircraft, control considerations should be addressed early to adequately define the aircraft configuration. In this case the peak actuator rate required by the feedback control system to recover from an initial disturbance was considered. The inclusion of this metric adds an extra dimension to the horizontal tail-sizing problem. The two-dimensional tail-sizing scissors plot is insufficient, and a natural extension is the tail-sizing design space. A conventional scissors plot can be recovered by viewing the intersection of the tail-sizing design space with a level plane representing peak actuator rate. The three-dimensional space allows the designer to assess the sensitivity of the location of the aft boundary to changes in actuator rate. The value added is in determining when small changes in the c.g. location result in large changes in the maximum actuator rate required.

A numerical algorithm was developed that provides the capability to quickly determine the tail-sizing design space for a given aircraft configuration. Using the tail-sizing design tool, the user can make adjustments to the aircraft definition and quantifiably assess the impact of the demands of the feedback control system on aircraft definition. As an example, the two changes in aircraft definition considered were the inclusion of canards in addition to a horizontal tail and the inclusion of the dynamics of the first symmetric bending mode. The influence of these factors on the tail-sizing design space for a representative model of a supersonic transport aircraft was quantified.

Numerical results suggest that canards provide a small benefit for a rigid-body model. Their use is more effective on a flexible-body model. The metric used to assess their effectiveness was the change in total horizontal control volume. In the example considered an aeroelastic model realized a reduction in total horizontal control volume of approximately 30% through the use of a canard. The rigid-body model realized a reduction in total horizontal control volume of approximately 10%.

Acknowledgment

This work was supported by NASA Langley Research Center under Contract L65444D.

References

[1] Kaminer, I., Howard, R., and Buttrill, C., "Development of Closed-Loop Tail-Sizing Criteria for a High Speed Civil Transport," *Journal of Aircraft*, Vol. 34, No. 5, 1997, pp. 658–664.

[2] Niewoehner, R. J., and Kaminer, I. I., "Integrated Aircraft–Controller Design Using Linear Matrix Inequalities," *Journal of Guidance, Control, and Dynamics*, Vol. 19, No. 2, 1996, pp. 445–452.

[3] Hallberg, E., "On Integrated Design of Plant, Control and Guidance Systems," Ph.D. Dissertation, Dept. of Aeronautics and Astronautics, Naval Postgraduate School, Monterey, CA, Sept. 1997.

[4] Ashkenas, I., Magdaleno, R., and McRuer, D., "Flight Control and Analysis Methods for Studying Flying and Ride Qualities of Flexible Transport Aircraft," NASA CR 172201, Aug. 1983.

[5] Etkin, B., and Reid, L., *Dynamics of Flight, Stability and Control*, Wiley, New York, 1996.

[6] Gahinet, P., Nemirovski, A., Laub, A. J., and Chilali, M., *LMI Control Toolbox*, MathWorks, Natick, MA, May 1995.

[7] Waszak, M., and Schmidt, D., "Flight Dynamics of Aeroelastic Vehicles," *Journal of Aircraft*, Vol. 25, No. 6, 1988, pp. 563–571.